A general method to compute numerical dispersion errors and its application to stretched meshes

4 authors, including:

Aleix Báez Vidal
Universitat Politècnica de Catalunya
13 PUBLICATIONS   66 CITATIONS

SEE PROFILE

F.Xavier Trias
Universitat Politècnica de Catalunya
95 PUBLICATIONS   1,157 CITATIONS

SEE PROFILE

Joaquim Rigola
Universitat Politècnica de Catalunya
121 PUBLICATIONS   794 CITATIONS

SEE PROFILE

Some of the authors of this publication are also working on these related projects:

Project   Mechanical Vapour Compression desalination system driven by renewable energy (GREENMVC) View project

Project   CleanSky Project: Multivariable Environmental Control System for Aircrafts (MULTIECS) View project

A general method to compute numerical dispersion errors and its application to stretched meshes

J. Ruano[a,*], A. Baez Vidal[a,*], F.X. Trias[a], J. Rigola[a]

[a]*Heat and Mass Transfer Technological Center (CTTC), Universitat Politècnica de Catalunya – BarcelonaTech (UPC) ETSEIAT, Colom 11, 08222, Terrassa, Barcelona, Spain*

Abstract

This article presents a new spectral analysis approach for dispersion error and a methodology to numerically evaluate it. In practice, this new analysis allows the numerical study of dispersion errors on all types of mesh and for multiple dimensions. Nonetheless, when mesh uniformity and one-dimensionality assumptions are imposed as in the classical method, the results of this new technique coincide with those of the classic method. We establish the theoretical basis of the approach, derive a numerical methodology to evaluate dispersion errors and assess the method after a set of numerical tests on non-uniform stretched meshes.

Keywords: dispersion, diffusion, numerical errors, wave propagation errors

1. Introduction

Computational Fluid Dynamics (CFD) is the branch of physics that computes and analyses numerical simulations that involve fluid flow. The branch of CFD that studies the generation and propagation of sound caused by fluid flow is known as Computational Aeroacoustics (CAA). In CAA, it is essential to keep accuracy to simulate the propagating speed of sound waves. Else, the interference patterns are erroneous and the simulations are irrelevant. The main scheme-depending factor affecting the simulated wave propagation velocity is the specific discretization of the differential operator of the equations ruling the fluid movement. In this regard, the classical dispersion error analysis [10] concludes that high order numerical schemes alleviate the committed propagation error.

The classical methodology applies on the transport term of the system of Partial Differential Equations modelling wave propagation. However, it requires this term to be in advective form. For example, for the Euler Equations, one should use their characteristics form, i.e., the fluxes are calculated after applying the chain rule for the derivatives

$$\frac{\partial}{\partial t}\boldsymbol{q} + \nabla \cdot \boldsymbol{f}(\boldsymbol{q}) = \frac{\partial}{\partial t}\boldsymbol{q} + J(\boldsymbol{f}, \boldsymbol{q}) \cdot \nabla \boldsymbol{q} = \boldsymbol{0}; \tag{1}$$

*Corresponding author

Email addresses: `jesusr@cttc.upc.edu` (J. Ruano), `aleix@cttc.upc.edu` (A. Baez Vidal), `xavi@cttc.upc.edu` (F.X. Trias), `quim@cttc.upc.edu` (J. Rigola)

where $\boldsymbol{q} \in \mathbb{R}^{D+2}$ are the fluid magnitudes, $\boldsymbol{f} \in \mathbb{R}^{D+2}$ Eulerian fluxes, $J(\boldsymbol{f}, \boldsymbol{q}) \in \mathbb{R}^{(D+2)\times(D+2)}$ the Jacobian $J_{ij} = \partial f_i / \partial q_j$ and D the number of dimensions of the model. Then, the term in the center of Eq.(1) is projected on a unitary orthonormal basis of the Euclidean space where it is defined and one obtains the set of locally decoupled wave equations on each of the characteristic variables

$$\frac{\partial}{\partial t} r_j + c_j \frac{\partial}{\partial s} r_j = 0, \qquad j \in [1, D+2], \tag{2}$$

where t is the time and s is a generic space coordinate. Then, the analysis studies the ratio between numerical approximations of $\partial r_j / \partial s$ and r_j in Eq.(2) when r_j are mono-modal sinusoids and the analytical values these ratios should take. These ratios are evaluated in the Fourier space by means of the Fourier Transform algorithm. The wave propagation speeds c_j in this procedure are assumed to be constant in space and time.

Tam et al. [16, 17] used the classical analysis to develop numerical methods that reduce such errors by following the relationship between wavenumber and wave speed propagation, i.e. the dispersion relation. The extracted conclusions of both analysis, summarized in Colonius [6], have favored the use of high order methods in wave propagation problems. For example, Bogey et al. [4] used high order schemes to aleviate the dispersion error [5] to simulate flow and acoustic fields of high-Reynolds jets. Shur et al. [14, 15] also used a fourth order central - fifth order upwind variant of the Roe scheme to compute the inviscid fluxes in their jets simulation. Bodony [3] compiled a list of several works in the field of jet-noise computation which used high order approximations of the convective term. Whereas previous authors solved Navier-Stokes equations to compute noise, Ewert [7] and Seo [12] solved additional differential equations. Nevertheless, they also used high order approximations of the transport term to reduce the dispersion.

However, the range of validity of the classical dispersion error analysis is limited due to the assumptions it lies on:

- Uniform mesh/spacing: The function at neighbour nodes, control volumes or points, is expressed as a shift of the function at the central node of the stencil.

- Linear wave propagation: The convective operator is linearized into the gradient operator multiplied by a constant propagation speed (c_j in Eq.(2) is constant).

- Linear schemes: The coefficients of the stencil are constant during the simulations and not dependent on the obtained fields, i.e., a linear discrete operator.

Consequently, the theoretical framework of [10, 16, 17] does not cover all the possible situations in CAA. In addition, no means to extend the validity of the analysis are given.

The limitations of the classical analysis become apparent when simulating flows in 2 or 3 space dimensions. Then, a common approach is to apply one stencil for each direction and assume that the overall method

2

reduces the overall dispersion error because each direction stencil does. However, wave propagation in 2D and 3D brings issues like anisotropy and wavenumber directionality that cannot be modelled in 1D and are forfeit when choosing or designing numerical schemes.

Another limitation of the classical analysis comes when trying to take into account the effect of non-linearity of convection on dispersion error. To do it, Pirozzoli [11] developed a different methodology based on a numerical single time step integration.

Finally, the classical analysis does not allow to study mesh non-uniformity in regard of the properties of the numerical schemes. Such analyses would have a great impact since most of the meshes for CAA simulations are stretched in the direction of wave propagation; see Bogey [4], Shur [14, 15] or Bodony [3]. Even in the case when the extracted conclusions were mesh dependant, a dispersion error analysis that accepted non-uniform discretizations would help to understand the behaviour of the differencing scheme on non-uniform meshes and designing meshes accordingly.

Only Trefethen [18] and Vichnevetsky [20] performed this kind of analysis examining how grid stretching and anisotropy, or non-constant coefficients affected the accuracy of wave propagation and generation of dispersive waves. The Fourier Transform of a function is the projection on the space of the eigenfunctions of the countinuous Laplacian operator [8]. Once the space is discretized, the discrete equivalent of the continuous Laplacian is a discrete Laplacian, and the equivalent of its eigenfunctions are now eigenvectors. Both sets of eigenfunctions and eigenvectors are orthogonal. When evaluating the eigenfunctions of the continuous Laplacian on a discretization, the resulting set of vectors are not orthogonal unless the discretization is uniform. The Discrete Fourier Transform (DFT) lies on this assumption. Henceforth, the DFT is not well fit for analysing dispersion errors on non evenly-spaced discretizations.

To sum up, the main reason for using high order methods to reduce dispersion error in wave propagation simulations seems to be weak when studying flow-depending operators, multiple dimensions or non-uniform meshes. Here we develop a new methodology to overcome the limitations of the classical approach. This opens the door to dispersion error analysis in any possible mesh. The presented methodology is tested in a Finite Volume Method (FVM) framework.

The rest of the paper is organized as follows: in section 2 the link between the classical approach used to study dispersion error and the present methodology is discussed as well as all the analytical derivation required. In section 3 we detail how to apply this alternative methodology. In section 4, a set of numerical tests are proposed and conducted. The results are latter analysed and commented. Finally, in section 5 the extracted conclusions of the whole paper are discussed.

2. Analytical derivation

Let $f(x) : \mathbb{R} \mapsto \mathbb{R}$ be a function that could be decomposed into a sum of sinusoids and

$$\widehat{f} = \int\limits_{-\infty}^{\infty} f(x)e^{-2\pi i x \alpha}\, dx, \tag{3}$$

its Fourier Transform. The Fourier Transform of the derivative

$$f' = \frac{d}{dx}f(x), \tag{4}$$

of f is:

$$\widehat{f'}(\alpha) = i\alpha\widehat{f}. \tag{5}$$

However, the previous expressions do not hold when the space is discretized. Taking a discretization of the physical space defined by $\Omega = \{\omega_1(x),\, \omega_2(x),\, \omega_3(x),\, \ldots, \omega_N(x)\}^T$, f is approximated with

$$f(x) \simeq \sum_{j=1}^{N} \omega_j(x)f_j = \Omega \cdot \boldsymbol{f}, \tag{6}$$

where the "N" scalars f_j are the components of the array $\boldsymbol{f} = \{f_1,\, f_2,\, f_3,\, \ldots, f_N\}^T \in \mathbb{R}^N$. If a Finite Difference discretization is selected, the different elements of Ω would be equal to:

$$\omega_i(x) = \begin{cases} 1 & \text{if} \quad x = x_i \\ \\ 0 & \text{elsewhere} \end{cases} \tag{7}$$

In case a Finite Volume approach is selected, with non-overlapping volumes, the elements of Ω would be:

$$\omega_i(x) = \begin{cases} 1 & \text{if} \quad x \in V_i \\ \\ 0 & \text{elsewhere} \end{cases} \tag{8}$$

Where V_i denotes the ith control volume of the discretization. Assuming the discretization is uniform and the physical space is 1D, one can approximate the derivative f' with

$$f'(x) \simeq \sum_{j=1}^{N} \omega_j(x) \sum_{k=1}^{N} a_{j,k}f_k, \tag{9}$$

The previous equation can be written in a matrix-vector form as:

$$f'(x) \simeq \Omega^T A\boldsymbol{f}, \tag{10}$$

where the matrix A stands for the discrete differential operator.

4

Applying the shifting theorem and the derivative theorem (Tam [16, 17]), the Fourier Transforms of f and the discrete approximation to its derivative are related with

$$\widehat{f'}(\alpha) \approx \frac{1}{\Delta x}\left[\sum_k a_k e^{ik\alpha\Delta x}\right]\widehat{f}(\alpha). \tag{11}$$

And the numerical wavenumber $\widetilde{\alpha}$ according to the classical analysis follows straighforwardly:

$$i\widetilde{\alpha}\widehat{f} = \frac{1}{\Delta x}\left[\sum_k a_k e^{ik\alpha\Delta x}\right]\widehat{f} \Longrightarrow \widetilde{\alpha} = \frac{-i}{\Delta x}\left[\sum_k a_k e^{ik\alpha\Delta x}\right]. \tag{12}$$

But this definition assumes a uniform 1D mesh. To broaden the concept of numerical wavenumber to non-uniform meshes where Eq.(11) does not apply, the eigenvalues of the derivative operator can be studied. More precisely, the differences between the analytical and numerical eigenvalues of the derivative operator. To extend the concept to non-uniform discretizations, we realize that the Fourier Transform projects functions into the space of eigenfunctions of the derivative operator of evenly distributed domains, i.e., Euclidean spaces or uniformly discretized domains. Thus, instead of projecting the function f in the space of sinusoids, we propose to project f into the space of eigenfunctions of the derivative operator, which does not coincide with sinusoids in non-uniform discretizations. Then, Eq.(5) must be rewritten as:

$$f'^\dagger(\lambda) = \lambda f^\dagger(\lambda), \tag{13}$$

where the projection, $()^\dagger$, is computed as:

$$\begin{aligned} f'^\dagger(\lambda) &= \int_{-\infty}^{\infty} f'(x)\cdot\beta(\lambda,x)\,dx; \\ f^\dagger(\lambda) &= \int_{-\infty}^{\infty} f(x)\cdot\beta(\lambda,x)\,dx, \end{aligned} \tag{14}$$

and β and λ are the appropiate set of eigenfunctions and eigenvalues extracted from the first-order derivative operator. If we let

$$\langle\xi\,|\,\psi\rangle_{\Omega_\mu} = \int_{\Omega_\mu}\xi(\mu)\overline{\psi}(\mu)\,d\mu. \tag{15}$$

be the inner product of $\{\xi,\psi\}\in\mathcal{L}^2(\Omega_\mu,\mu)$, where $\mathcal{L}^2(\Omega_\mu,\mu)$ is the space of square Lebesgue-integrable functions $\psi:\Omega_\mu\subset\mathbb{R}\mapsto\mathbb{C}$ and $\overline{\psi}$ the complex conjugate of ψ. We can rewrite the projections in a more compact form:

$$\begin{aligned} f'^\dagger(\lambda) &= \langle f'\,|\,\beta\rangle_{\Omega_x}; \\ f^\dagger(\lambda) &= \langle f\,|\,\beta\rangle_{\Omega_x}. \end{aligned} \tag{16}$$

Once discretized, an implicit relation between the numerical eigenvalue and the analytical one is found:

$$\widetilde{\lambda} = \frac{\widetilde{f'^\dagger}}{\widetilde{f^\dagger}} = \frac{\langle A\boldsymbol{f}\,|\,\boldsymbol{\beta}\rangle}{\langle\boldsymbol{f}\,|\,\boldsymbol{\beta}\rangle}, \tag{17}$$

5

where the discrete inner product is defined as:

$$\langle \boldsymbol{\phi} \,|\, \boldsymbol{\psi} \rangle = \sum_{j=1}^{N} \phi_j \sum_{k=1}^{N} \langle \omega_j \,|\, \omega_k \rangle_{\Omega_x} \overline{\psi_k}. \tag{18}$$

We remark that ω_j and ω_k are the j and k terms of the discretization Ω defined at the beginning of this section.

Both methodologies, the classical and that defined in Eq.(17), assume that the derivative can be explicitly projected into a selected space of functions and depends linearly on the original f. For more complicated derivation processes, e.g. non-linear differential operators, these expressions are not valid. Consequently, another method is proposed.

Namely, let $\Phi = \{\phi_{-N}(x), \phi_{-N+1}(x), \ldots \phi_{-1}(x), \phi_0(x), \phi_1(x), \phi_2(x), \ldots \phi_N(x)\}$ be an orthonormal basis of functions of $\Omega_x \subset \mathbb{R}$, i.e,

$$\langle \phi_m \,|\, \phi_n \rangle_{\Omega_x} = \delta_{mn}, \tag{19}$$

where δ_{mn} is the Kronecker's delta.

One can thus define a mapping $T : \mathcal{L}^2(\Omega_x, x) \mapsto \mathbb{C}^{2N+1}$; $T : f(x) \mapsto (\alpha_m) \in \mathbb{C}^{2N+1}$, where

$$\alpha_m = \langle f \,|\, \phi_m \rangle_{\Omega_x} = \int_{\Omega_x} f(x) \overline{\phi_m}(x) \, dx, \tag{20}$$

is the projection of $f(x)$ onto the m function Φ. Under the pertinent smoothness of f criterion,

$$f(x) \simeq S_N = \sum_{m=-N}^{N} \alpha_m \phi_m(x); \quad \lim_{N \to \infty} S_N = f(x). \tag{21}$$

This defines the inverse mapping $T^{-1} : \mathbb{C}^{2N+1} \mapsto \mathcal{L}^2(\Omega_x, x)$, $T : (\alpha_m) \in \mathbb{C}^{2N+1} \mapsto f(x)$.

The derivative $f' = \frac{d}{dx} f(x)$ can also be expressed in terms of its projection on the set of functions of Φ:

$$f'(x) \simeq S'_N = \sum_{m=-N}^{N} \alpha_m \phi'_m(x) \simeq \sum_{m=-N}^{N} \alpha_m \sum_{n=-N}^{N} \gamma_{mn} \, \phi_n(x), \tag{22}$$

where

$$\gamma_{mn} = \langle \phi'_m \,|\, \phi_n \rangle_{\Omega_x}. \tag{23}$$

This holds on the orthonormality of the functions of Φ:

$$\gamma_{mn} = \langle \phi'_m \,|\, \phi_n \rangle_{\Omega_x} = \left\langle \sum_{p=-N}^{N} \gamma_{mp} \, \phi_p(x) \,|\, \phi_n \right\rangle_{\Omega_x} = \sum_{p=-N}^{N} \gamma_{mp} \langle \phi_p \,|\, \phi_n \rangle_{\Omega_x} = \sum_{p=-N}^{N} \gamma_{mp} \delta_{pn} = \gamma_{mn}. \tag{24}$$

With these definitions, γ_{mn} are the elements of a matrix $\Gamma \in \mathbb{C}^{2N+1 \times 2N+1}$ and the projections of the derivatives of ϕ_m with respect to "x" on ϕ_n. Γ characteristics are determined by the selected basis of

6

functions Φ and the properties of the derivative operator. Assuming null contributions from boundaries and integrating by parts, it is straightforward to show that the derivative operator is skew-Hermitian with respect to the inner product of Eq.(15), i.e.,

$$\left\langle \frac{d}{dx}\xi \,|\, \psi \right\rangle_{\Omega_x} = -\left\langle \xi \,|\, \frac{d}{dx}\psi \right\rangle_{\Omega_x}. \tag{25}$$

Thus, Γ should be skew-Hermitian too.

Using an approximate derivative operator $\widetilde{\frac{d}{dx}}(\cdot)$, one gets $\widetilde{\Gamma} \in \mathbb{C}^{2N+1 \times 2N+1}$ instead. Making a parallelism with Eq.(17), the errors associated with using approximate differential operators to approximate derivatives are the deviations of $\widetilde{\gamma}_{mn}$ from γ_{mn}. Finally, to ease the analysis, Φ can be chosen such that Γ is diagonal and known, i.e., ϕ_m is an eigenfunction of the derivative. Then, the possible errors in $\widetilde{\Gamma}$ are:

- $\widetilde{\gamma}_{mn} \neq 0$ if $m \neq n$,

- $Re(\widetilde{\gamma}_{mm}) \neq 0$, and

- $\dfrac{Im(\widetilde{\gamma}_{mm})}{\lambda_m} \neq 1$,

where $\lambda_m \in \mathbb{I}$ is the eigenvalue of the derivative on ϕ_m. A methodology to compute these errors is described in the next section.

3. Methodology

When functions are approximated with discretizations as in Eq.(6) to operate with arrays of scalars, the differential operators of the equations describing some physical phenomena should be approximated accordingly. For example, if $\boldsymbol{f}$ is the discrete representation of $f(x)$ on $\Omega = \{\omega_1(x),\, \omega_2(x),\, \omega_3(x),\, \ldots, \omega_N(x)\}$ as defined in Eq.(6), the discrete representation of an approximation to its derivative $\boldsymbol{f'}$ is represented on $W = \{w_1(x),\, w_2(x),\, w_3(x),\, \ldots, w_M(x)\}$. The different discretizations methodologies of CFD contemplate $W \neq \Omega$. However it is common to project the calculated derivatives onto the original Ω (see, e.g. [19]) in following computation steps. Here, we focus on the compound process $A : \mathbb{R}^N \mapsto \mathbb{R}^N$, i.e. the approximation to the derivative $\boldsymbol{f} \mapsto A(\boldsymbol{f})$ and its projection onto Ω. Since differential operators are linear, their discrete counterparts should be linear too. Therefore, $A(\boldsymbol{f}) = A\boldsymbol{f}$; $A \in \mathbb{R}^{N \times N}$. Splitting A into the Hermitian, D, and skew-Hermitian, C, parts [1],

$$C = \frac{1}{2}(A - A^*); \tag{26}$$

$$D = \frac{1}{2}(A + A^*); \tag{27}$$

$$A = C + D, \tag{28}$$

7

where $(\cdot)^*$ indicates the conjugate transpose. The previous matrices have interesting properties regarding the inner product:

$$
\begin{aligned}
\langle C\boldsymbol{\psi} \,|\, \boldsymbol{\psi} \rangle &\in \mathbb{I} \\
\langle D\boldsymbol{\psi} \,|\, \boldsymbol{\psi} \rangle &\in \mathbb{R} \\
\langle C\boldsymbol{\psi} \,|\, \boldsymbol{\eta} \rangle &= -\langle \boldsymbol{\psi} \,|\, C\boldsymbol{\eta} \rangle \\
\langle D\boldsymbol{\psi} \,|\, \boldsymbol{\eta} \rangle &= \langle \boldsymbol{\psi} \,|\, D\boldsymbol{\eta} \rangle,
\end{aligned}
\tag{29}
$$

where $\{\boldsymbol{\psi}, \boldsymbol{\eta}\} \in \mathbb{C}^N$.

Both matrices C and D are related, respectively, to the real and the imaginary part of the γ scalars of Eq.(23). For a given discretization, these scalars can be numerically calculated:

$$
\begin{aligned}
\widetilde{\gamma}_{mn} &= \langle A\boldsymbol{\phi_m} \,|\, \boldsymbol{\phi_n} \rangle \\
\widetilde{\gamma}_{mn}^C &= Im(\widetilde{\gamma}_{mn}) = \langle C\boldsymbol{\phi_m} \,|\, \boldsymbol{\phi_n} \rangle \\
\widetilde{\gamma}_{mn}^D &= Re(\widetilde{\gamma}_{mn}) = \langle D\boldsymbol{\phi_m} \,|\, \boldsymbol{\phi_n} \rangle.
\end{aligned}
\tag{30}
$$

This development holds because Φ is orthonormal and due to the nature of the skew and Hermitian operators. They can be calculated from A:

$$
\begin{aligned}
\widetilde{\gamma}_{mn}^C &= \langle C\boldsymbol{\phi_m} \,|\, \boldsymbol{\phi_n} \rangle = \frac{\langle A\boldsymbol{\phi_m} \,|\, \boldsymbol{\phi_n} \rangle - \langle \boldsymbol{\phi_m} \,|\, A\boldsymbol{\phi_n} \rangle}{2} \\
\widetilde{\gamma}_{mn}^D &= \langle D\boldsymbol{\phi_m} \,|\, \boldsymbol{\phi_n} \rangle = \frac{\langle A\boldsymbol{\phi_m} \,|\, \boldsymbol{\phi_n} \rangle + \langle \boldsymbol{\phi_m} \,|\, A\boldsymbol{\phi_n} \rangle}{2},
\end{aligned}
\tag{31}
$$

where the values of γ_{mn} are the different elements of the matrix Γ. To simplify the analysis, we propose to compute the root mean square of the second index of the values of γ,

$$
\begin{aligned}
\widetilde{\lambda}_m^C &= \sqrt{\sum_n \left(\frac{\langle A\boldsymbol{\phi_m} \,|\, \boldsymbol{\phi_n} \rangle - \langle \boldsymbol{\phi_n} \,|\, A\boldsymbol{\phi_m} \rangle}{2} \right)^2} \\
\widetilde{\lambda}_m^D &= \sqrt{\sum_n \left(\frac{\langle A\boldsymbol{\phi_m} \,|\, \boldsymbol{\phi_n} \rangle + \langle \boldsymbol{\phi_n} \,|\, A\boldsymbol{\phi_m} \rangle}{2} \right)^2}.
\end{aligned}
\tag{32}
$$

This procedure allows a faster comparison between the analytical value and the recovered numerical ones. Thus, if the recovered $\widetilde{\lambda}_m^D$ is not null, the differential operator will have diffusive behavior. If the ratio between $|\widetilde{\gamma}_{mm}|$ and $\widetilde{\lambda}_m^C$ is lesser than the unity, then values of $\widetilde{\gamma}_{mn}$ which should be zero will have a non-zero value. And finally, the ratio between $\widetilde{\gamma}_{mm}$ and the reference parameter indicate the deviation of the numerical discretization from its expected value.

In summary, given a set of approximations of differenciating operators $\{A_1, A_2, \ldots, A_P\}$, their dispersion properties on a representative mesh can be compared after computing the quantites $\widetilde{\lambda}_m^{C_j}$ and $\widetilde{\lambda}_m^{D_j}$ for each element ϕ_m of an orthonormal basis and discrete operator A_j. The following subsections address the evaluation of A_j and the selection of an appropiate orthonormal basis Φ.

3.1. Evaluating the gradient

To evaluate the approximations of the derivative operators we propose to substitute Eq.(2) with

$$
\frac{\partial r_j}{\partial t} + C(c_j, r_j) = 0, \qquad j \in [1, D+2];
\tag{33}
$$

8

where $C(c_j, r_j)$ is the convection operator on r_j. After this, approximations of derivative operators can be easily obtained with $c_j = 1$. Notice that in the continuous space or with constant c_j Eqs. (2) and (33) are equivalent. In practical simulations, the discrete convective operator is an isomorphism, i.e. $C : \Omega \mapsto \Omega$. Hence, this resolves the eventual problem of the different basis pointed out in former paragraphs of this section. Furthermore, Eq.(33) is advantageous in discretizations where c_j is not constant. In fact, in the Euler Equations in form of Eq.(33), $c_j : \mathbb{R}^{D+2} \mapsto \mathbb{R}$; $c_j(\boldsymbol{r})$ and their spatial variations can only be neglected for small perturbations (e.g. acoustics).

However, this assumption does not hold when simulating hydrodynamic regions. In these regions, the spatial variations of $\boldsymbol{r}$ are of the same order of magnitude and spatial variatons of c_j cannot be neglected. Nonetheless, the literature shows how low-dispersion arguments based on the classical methodology have been employed to support using high-order numerical schemes in these regions. We expect that the dispersion analysis developed here with the derivatives computed via Eq.(33) will allow comparing schemes in hydrodynamic regions.

3.2. Selection of an orthonormal basis

The method described above has to be applied on an appropriate orthonormal basis of the discrete fields, Φ. The classical analysis [10, 16, 17] performs the dispersion error analysis on uniform structured meshes. On them, it is straightforward to use the projections of sinusoids on the canonical basis Ω^0, i.e., define a change of basis of the type $B : \mathbb{R}^N \mapsto \mathbb{R}^N$. For example, in Finite Differences or Finite Volumes formulations, one can use $b_{jk} = \left\langle \sin(jx) \, | \, \omega_k^0 \right\rangle_{\Omega_x}$. However, in non-uniform or unstructured meshes, this procedure does not generate orthonormal basis.

For these cases, we propose to use the eigenvectors of discrete Laplacian operators defined on such meshes. This basis is used in signal analysis and related fields (see Shuman et al.[13]). Among others, the properties of the eigenvectors of the discrete Laplacian operator are:

- The eigenvectors are orthonormal.

- In evenly spaced domains, the eigenvectors are discretized sinusoids.

- In the continuous limit, its eigenvectors and eigenvalues collapse into the eigenfunctions of its continuous counterpart, i.e. sinusoids.

- They retain the concept of mesh connectivity.

Furthermore,

$$L = G^*G, \tag{34}$$

where $L \in \mathbb{R}^{N \times N}$ is a discrete Laplacian, $G \in \mathbb{R}^{M \times N}$ a discrete gradient (see [2]) and G^* the conjugate-transpose of G. It is important to notice that G is not necessarily the differenciating operator on which the

Figure 1: Examples of discrete eigenvectors in two-dimensional structured uniform mesh. Left: low eigenvalue associated, right: high eigenvalue associated.

dispersion error analysis is to be conducted but a differencing operator that holds the equality. Actually, Φ should be independent of the scheme under study to allow comparisons if several of them will be tested.

The Singular Value Decomposition of G relates its right-eigenvectors $\{\boldsymbol{g_1}, \boldsymbol{g_2}, \ldots, \boldsymbol{g_N}\}$ and singular values $\{g_1, g_2, \ldots, g_N\}$ with the eigenvectors $\{\boldsymbol{l_1}, \boldsymbol{l_2}, \ldots, \boldsymbol{l_N}\}$ and eigenvalues of $\{l_1, l_2, \ldots, l_N\}$ of L. Specifically, $g_n = \sqrt{l_n}$ and $\boldsymbol{g_n} = \boldsymbol{l_n}$.

Thus, any scheme under analysis will be compared to a reference gradient. With this, we propose to calculate the quantities of Eq.(32) with $\Phi = \{\boldsymbol{l_1}, \boldsymbol{l_2}, \ldots, \boldsymbol{l_N}\}$ and $\lambda_j = \sqrt{l_j}$ for all $j \in [1, N]$.

The discrete eigenvectors of a 2nd order discrete symmetric Laplacian operator are shown in figures 1-3. To ensure symmetry of the obtained matrix, this Laplacian has been constructed as:

$$L = \sum_{p \in Nb} a_p(\phi_p - \phi_o) = 0; \qquad a_p = \frac{A_{op}}{\overrightarrow{d_{op}}\overrightarrow{n_{op}}\dfrac{V_p + V_o}{2}}, \tag{35}$$

where A_{op} is the intersection area between volumes o and p, $\overrightarrow{n_{op}}$ its normal vector, $\overrightarrow{d_{op}}$ the distance between centroids and V_p and V_o, the volumes p and o. Nb indicates the number of neighbours that surround control volume o.

The results resemble, into some extent, a discrete sinusoid; this is more obvious when low modes are selected. When higher modes are selected, as on the figures on the right, this similarity can be lost if non-uniform, or non-structured meshes are used.

3.3. Studying sinusoids or other functions

It may be argued that the present methodology is that the discrete eigenvalues of L are not directly related with waves in the physical, continuous, space. However, the closer the discrete L approximates the

10

Figure 2: Examples of discrete eigenvectors in two-dimensional structured non-uniform mesh. Left: low eigenvalue associated, right: high eigenvalue associated.
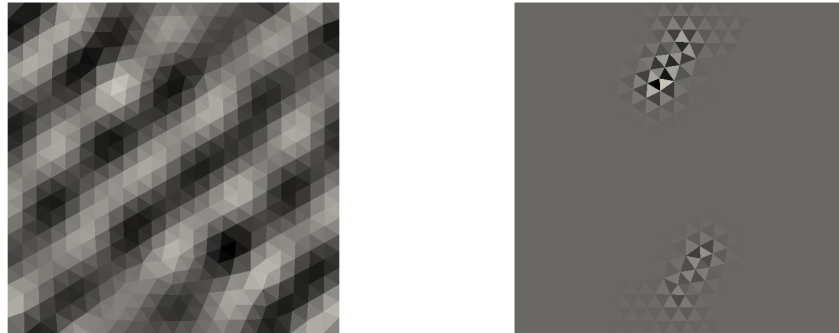

Figure 3: Examples of discrete eigenvectors in two-dimensional unstructured mesh. Left: low eigenvalue associated, right: high eigenvalue associated.

continuous ∇^2, the closer are its eigenvalues and eigenvectors to resemble physical waves. Put short, using high order L resolves the problem, at least for long wavelengths with respect to the mesh characteristic spacing. But still, the user of the present methodology does not have a strict control of the wavelengths that will be the eigenvalues of L on a mesh.

The following method allow to evaluate dispersion errors for any function f and, in particular, a sinusoid with wavenumber "k", e.g., $f(k, x) = \sin(kx)$. Expressing f on Ω, $f(k, x) \simeq \sum_m a(k)_m \phi_m(x)$, with $a(k)_m = \langle f | \phi_m \rangle_{\Omega_x}$, which are the coordinates of the sinusiod function in the eigenvectors basis. The derivative is approximated with

$$f'(k, x) \simeq \frac{d}{dx} \sum_m a(k)_m \phi_m(x) = \sum_m a(k)_m \phi'_m(x) = \sum_m a(k)_m \sum_n \gamma_{mn} \phi_n(x), \tag{36}$$

We can compute an approximation to the classical dispersion error:

$$S(k, l) = \left\langle \widetilde{f'}(k, x) \,|\, f(l, x) \right\rangle_{\Omega_x} \simeq \left\langle \widetilde{\Gamma} \boldsymbol{a}(k) \,|\, \boldsymbol{a}(l) \right\rangle. \tag{37}$$

where $\widetilde{\Gamma}$ is defined as in Eq.(31). As a particular case, when l is equal to k, the above definition becomes the usual expression of dispersion error on evenly distributed meshes, i.e. how the derivative of a mode projects in the same mode:

$$S(k, k) = \left\langle \widetilde{f'}(k, x) \,|\, f(k, x) \right\rangle_{\Omega_x} \simeq \left\langle \widetilde{\Gamma} \boldsymbol{a}(k) \,|\, \boldsymbol{a}(k) \right\rangle. \tag{38}$$

Thus, the presented methodology is able to numerically approximate the results of classical analysis on general meshes, whereas the classical analysis cannot. The same numerical procedure allows to study the projection of the selected eigenvectors into any function of interest.

4. Numerical tests

The set of numerical experiments reported here illustrates the use of the developed methodology. We focus on stretched structured meshes as this type of meshes is a common practice that allows limiting the total mesh sizes and the associated computing cost and time in CAA. It allows, among others, a controlled refinement near walls or zones where a smaller mesh size is required without compromising the total amount of mesh nodes. However, a variation of the mesh size introduces errors that can potentially lead to instabilities. Estimating the magnitude of these errors before running a simulations allows designing of the simulations with the desired precision and accuracy.

The selected experiments consist of comparing dispersion errors of approximate derivatives on non-uniform structured 1D meshes with increasing degree of constant volume growth ratio. The test functions used to compute dispersion error are the discrete eigenvectors computed from the discrete Laplacian. The Laplacian is discretized as in Eq.(35), following a second order approximation of the differential operator,

ensuring symmetry of the obtained matrix, and with periodic boundary conditions. Once constructed, the eigenvalues and eigenvectors of the matrix, the discrete Laplacian matrix, are calculated by means of QR reduction algorithm present in GNU scientific library package [9]. The obtained test functions are then convected by using a second-order Symmetry Preserving approach of the discrete transport term of Navier Stokes equations. This term is linearized, i.e. constant advection velocity, in order to compare the presented method with the classical one due to the fact the latter implies a linear convective term. This means the studied convective term in one direction is:

$$C((1,0,0), \boldsymbol{\phi})_i = \frac{d}{dx}\boldsymbol{\phi}_i. \tag{39}$$

And its discrete counterpart in a Finite Volume framework:

$$\frac{d}{dx}\boldsymbol{\phi}_i \simeq \frac{1}{V_i}\sum_{f \in V_i} \phi_f A_f n_x. \tag{40}$$

Due to the fact a second-order Symmetry Preserving discretization has been selected, the value ϕ_f is equal to $\frac{1}{2}(\boldsymbol{\phi}_i + \boldsymbol{\phi}_{nb})$. Once advected, the matrix $\hat{\Gamma}$ is constructed following Eq.(31). In this case, having selected a conservative and non-diffusive discretization, the terms related to $\widetilde{\gamma}_{mn}^D$ are null. The final step of the procedure consists in calculating the dispersion characteristics in the sinusoids base by means of Eqs.(38) and (37). These values constitute the elements of matrix $S \in \mathbb{C}^{N \times N}$.

The meshes for the tests are 1D stretched meshes. The total size of the domain is the same in all the meshes and tests. The errors commited with the stretched meshes are compared with those commited with a uniform, cartesian 1D mesh. The range of studied wavenumbers is $\nu = [0 : k_{Max}] = [0 : 2\pi/\lambda_{Min}]$; being λ_{Min} the minimum studied wavelength and equal to $2\Delta x_{Min}$. Δx_{Min} the minimum cell size of the mesh. The volume size of the uniform mesh is the minimum volume size of the stretched ones; thus all meshes share the same maximum studied wavenumber. The characteristics of these meshes are reported in table 1 and some of them are shown in figure 4.

Figure 5 approximates the classical analysis: it shows the diagonal part of the recovered S matrix. Due to the fact a Symmetry Preserving discretization has been used these values are purely imaginary. For the uniform mesh, the analysis gives the same results as the classical analysis of Tam [17] and Lele [10]. This was expected because for structured meshes with periodic boundary conditions the discrete gradient operator can be expressed as a circulant matrix. Eigenvectors of these matrices are known to be discrete sinusoids. The results of the stretches meshes provide new insight in dispersion errors as this kind of result is innovative.

First, for the selected range of wavenumbers the stretched meshes exhibit reflections, or a change in the sign of the propagating wavenumber, at mid-to-higher wavenumbers. These reflections occur before, in a lesser wavenumber, in highly stretched than in slightly stretched meshes. Another immediate result extracted from figure 5 is that stretched meshes introduce an intermediate frequency on the positive side of

13

Δx_{Min}	Δx_{Max}	Volume growth ratio	Number of volumes	Mesh savings [%]
0.015625	0.015625	1.0	64	0
0.015625	0.018147	1.005	60	6.25
0.015625	0.020645	1.01	56	12.5
0.015625	0.023356	1.015	54	15.625
0.015625	0.025634	1.02	50	21.875
0.015625	0.028261	1.025	48	25
0.015625	0.030837	1.03	46	28.125
0.015625	0.033305	1.035	44	31.25
0.015625	0.037030	1.04	44	31.25
0.015625	0.039379	1.045	42	34.375
0.015625	0.041458	1.05	40	37.5

Table 1: Mesh characteristics.

Figure 4: Some of the used meshes. From top to bottom: from uniform mesh to 5% stretching with increments of 1%.
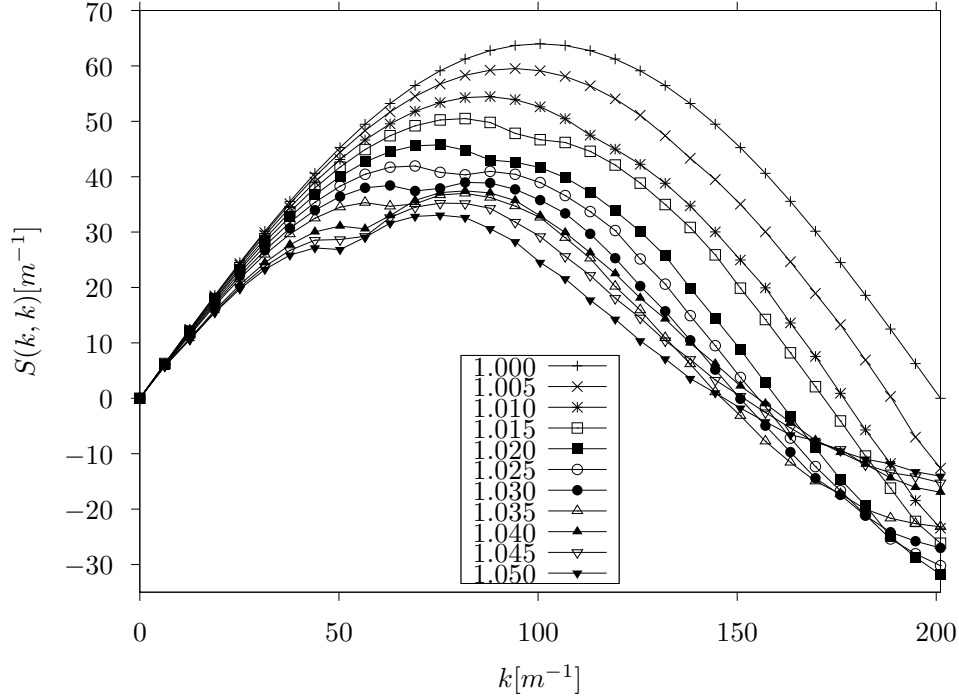
Figure 5: Diagonal terms vs imposed wavenumber in sinusoids space for different ratios.

the plot at which an inflection point appears. Later it will be discussed the relation of this kind of frequency with dimensional aspects of the mesh.

Figure 6 includes the effects of the off-diagonal terms of S, where the root mean square of the row elements is presented. This parameter is the equivalent of $\lambda(m)$ presented in Eq.(32) but in the space of sinusoids. As it can be seen, the shape of the plots is different from those in figure 5; these differences are enlarged at higher strecthing ratios. If figures 6 and 5 are different this means that other elements than the diagonal appear. Therefore, the recovered modes are composed of various frequencies instead of a single one, which should be only the diagonal term.

How the recovered mode, using the presented method, is composed of different modes is illustrated in figures 7 and 8, the uniform and mesh stretched a 5%. In the figures we use modes instead of frequencies, distinguishing between sinus and cosinus in order to show that even modes, i.e. sinus, project onto odd modes, cosinus, and viceversa. Ideally, the matrices of the figures should be diagonal, mode 'j' derivated projects into mode '$j+1$' or '$j-1$' and viceversa, and skew-symmetric.

As can be seen, only the uniform mesh provides a diagonal matrix. Stretched meshes provide additional off-diagonal terms. This means that the modes obtained when deriving in stretched meshes are composed of various modes instead a single one. The presence of these off-diagonal terms also explains why figures 5 and 6 are not identical.
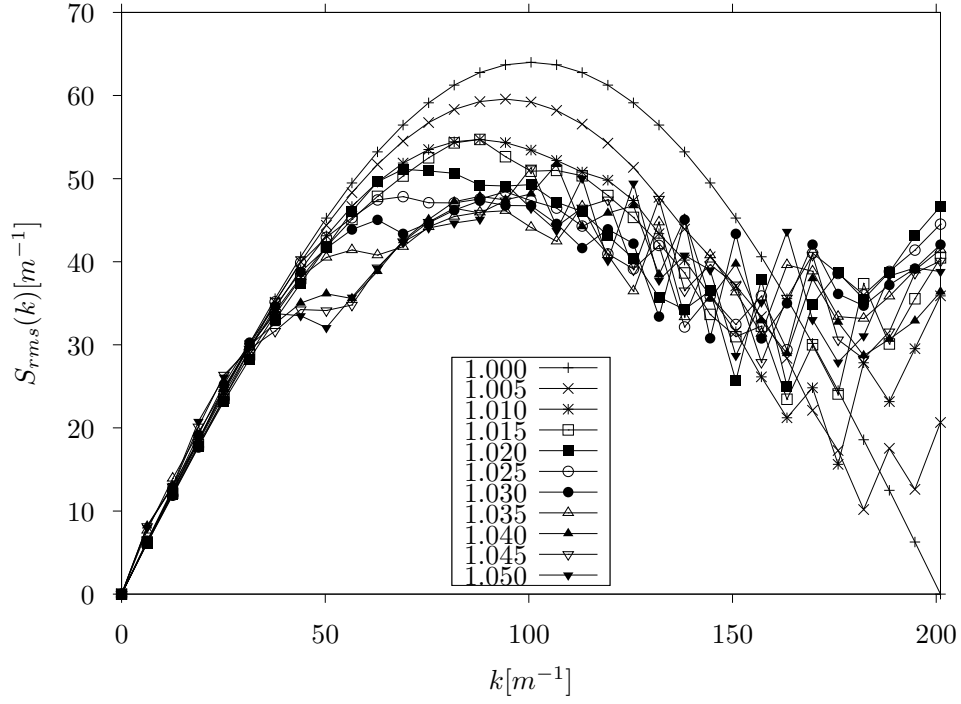
15

Figure 6: $\widetilde{\lambda}$ vs imposed wavenumber in sinusoids space for different ratios.
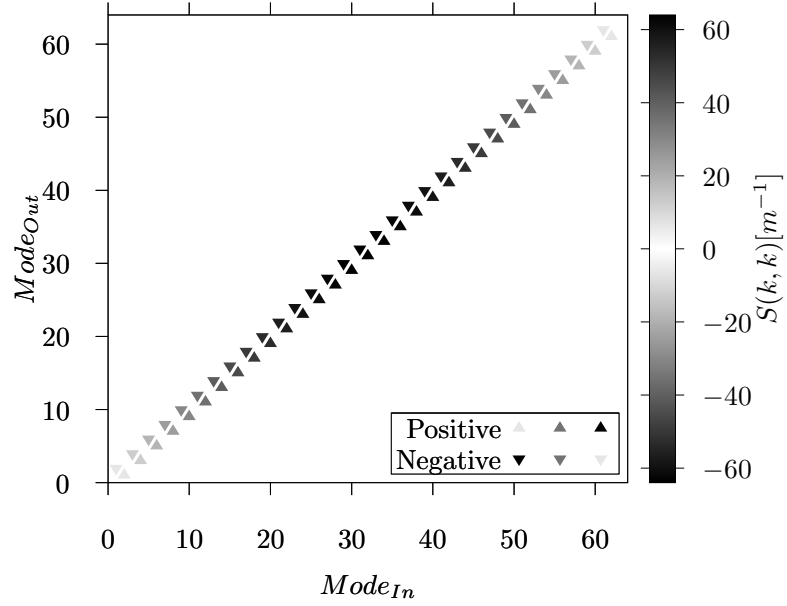

Figure 7: Dispersion matrix in sinusoids space for uniform mesh. Input mode in the horizontal axis and recovered mode of the derivative in the vertical axis.
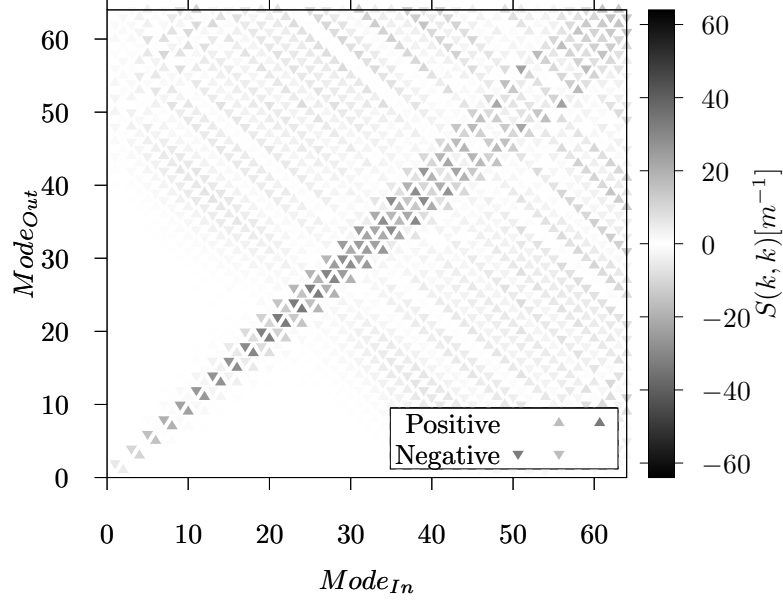
Figure 8: Dispersion matrix in sinusoids space for stretched mesh (ratio 1.05). Input mode in the horizontal axis and recovered mode of the derivative in the vertical axis.

In order to help understanding the mechanisms that happen during all the process, we include two new different plots:

- First, the equivalent of figures 5 and 6 but in the space of eigenvectors instead of the space of sinusoids, i.e. the values of Eq.(32). This will allow to study just the derivation process without involving a change of basis.

- Some values of $\boldsymbol{a}(k)$ at different meshes, which are the coordinates the sinusiod function in the eigenvectors basis, i.e. how a sinus of specific frequency is composed of several eigenmodes. This will help to understand how frequencies are composed of the different eigenmodes.

Previously it has been commented the existence of an intermediate frequency in figure 5. It is difficult to relate the frecuency in this plot, and even quantify it, to dimensional aspects of the mesh. However, in figure 9 this frequency, or eigenvalue in this figure, is more easily quantified. As can be seen, all the curves present a sudden decay and then a stabilization. The eigenvalue at which the decay transitions into stabilization has been found to be equal to $\frac{2}{\Delta x_{Max}}$ for each mesh.

In figure 10 the value of λ of Eq.(32) is plotted. This figure is slightly different from figure 9 for stretched meshes. This means that off-diagonal terms appear in matrix Γ; thus eigenmodes recovered after derivating are composed of various input eigenmodes instead of a single one. Consequently, one of the reasons because
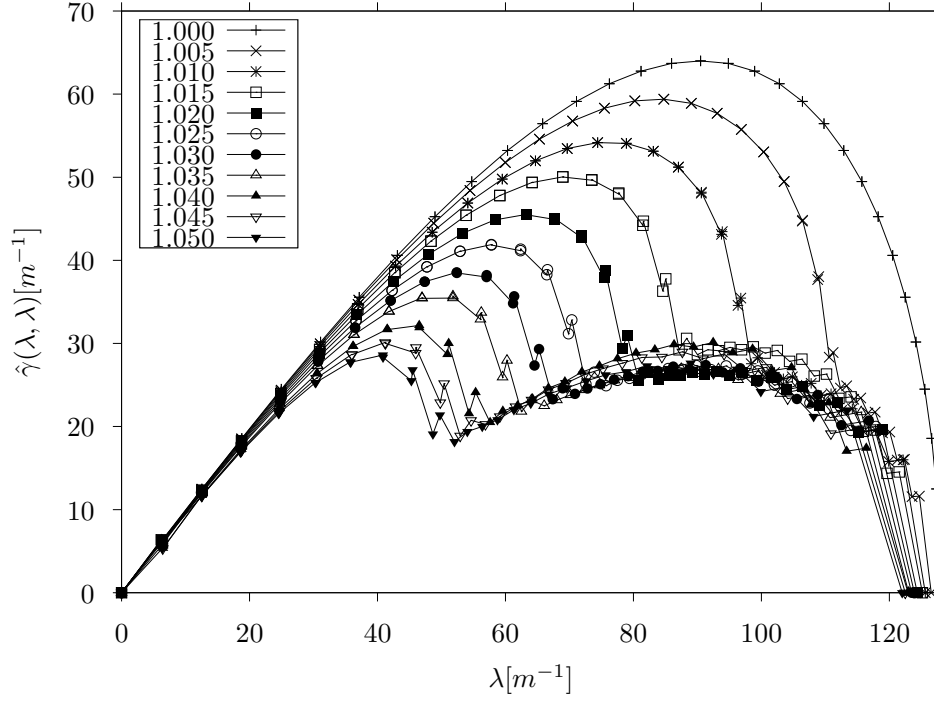
17

Figure 9: Diagonal terms vs imposed eigenvalue in eigenvectors space for different ratios.
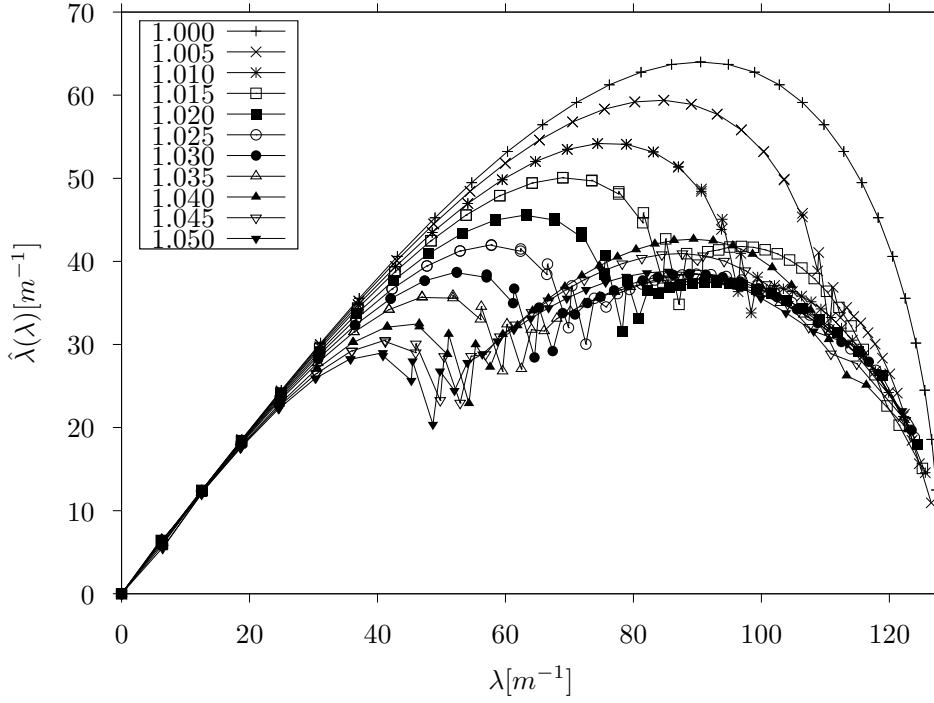

Figure 10: $\widetilde{\lambda}$ vs imposed eigenvalue in eigenvectors space for different ratios.
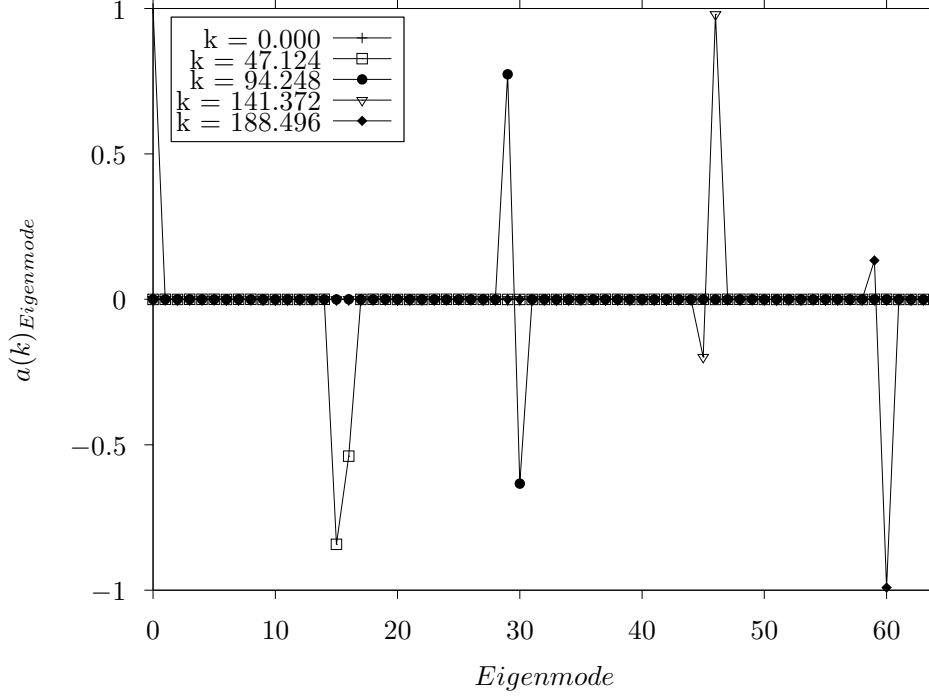
Figure 11: $\boldsymbol{a}(k)$ at different wavenumbers k for uniform mesh.

figure 8 is not diagonal occurs during the derivation process.

The other reason which will produce non-diagonal matrices will be that during the projection onto the sinusoid space the operation introduces off-diagonal terms. A single frequency composed of very different eigenmodes will propagate the information of these modes in a very sparse way, i.e. off-diagonal terms when computing $S(k, l)$.

As can be seen in figure 11, each frequency is represented by a single mode or by two consecutive in the worst case. This means each frequency is related to very few eigenmodes. On the other hand, figure 12 shows that each frequency is composed of a large amount of different eigenmodes; the higher the wavenumber, higher the number of eigenmodes that compose this frequency. Consequently, during the basis change using stretched meshes, the information contained in matrix $\hat{\Gamma}$ is further dispersed.

5. Conclusions

We have developed an alternative methodology to compute the dispersion error not restricted to uniform meshes. Due to the fact that the presented method does not require mesh uniformity, or more generaly a structured distribution of nodes, it has been tested using uniform and non-uniform structured meshes. The obtained results in uniform mesh are the same obtained by Tam [17] and Lele [10]; thus, the usual approach collapse on the current method when uniform meshes are used. The obtained results indicate that stretched
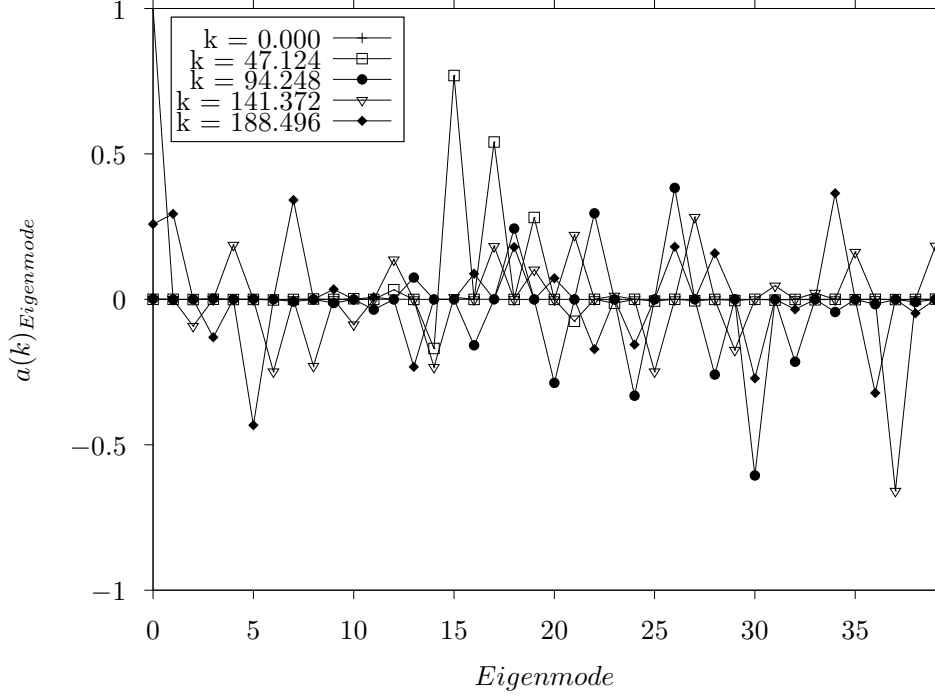
Figure 12: $\boldsymbol{a}(k)$ at different wavenumbers k for mesh with 5% stretching.

meshes, even with small values around 3-5% degrade the solution significantly. Thus, the usage of smaller values is highly recommended, as pointed by Shur [14] or Bogey [5] by means of the range of validity of their numerical results. It also has been computed how non-uniform stretched meshes induce projection on other frequencies. This implies that the frequency of the approximate derivative is composed by several frequencies rather than a unique mode. Additionally, it has been observed that the projection onto other frequencies performs through two mechanisms in stretched meshes:

- First, during the derivation process if the set of eigenvectors are not the eigenvectors of the discrete convective operator.

- Second, when projecting into the space of sinusoids and dispersing the information of the different eigenmodes into more frequencies.

It is hoped that the current approach will help to develop optimized schemes and selecting more appropiate ones taking into account different mesh geometries. We also hope this analysis to be useful to design mesh stretching strategies that reduce dispersion errors.

On a further work, we plan to use this method to test more differential schemes. Since non-linearity of the differential operator is not a requirement of the developed methodology, the analysis will be conducted on non-linear schemes.

Acknowledgements

References

References

[1] L. Beilina, E. Karchevskii, and M. Karchevskii. *Numerical Linear Algebra: Theory and Applications*. Springer, 2017.

[2] P. B. Bochev and J. M. Hyman. *Principles of mimetic discretizations of differential operators*. Springer, 2006.

[3] D. J. Bodony and S. K. Lele. Current status of jet noise predictions using large-eddy simulation. *AIAA journal*, 46(2):364–380, 2008.

[4] C. Bogey. Grid sensitivity of flow field and noise of high-reynolds-number jets computed by large-eddy simulation. *International Journal of Aeroacoustics*, 17(4-5):399–424, 2018.

[5] C. Bogey and C. Bailly. A family of low dispersive and low dissipative explicit schemes for flow and noise computations. *Journal of Computational physics*, 194(1):194–214, 2004.

[6] T. Colonius and S. K. Lele. Computational aeroacoustics: progress on nonlinear problems of sound generation. *Progress in Aerospace sciences*, 40(6):345–416, 2004.

[7] R. Ewert and W. Schröder. Acoustic perturbation equations based on flow decomposition via source filtering. *Journal of Computational Physics*, 188(2):365–398, 2003.

[8] J. Fourier. *Theorie analytique de la chaleur, par M. Fourier*. Chez Firmin Didot, père et fils, 1822.

[9] M. Galassi, J. Davies, J. Theiler, B. Gough, G. Jungman, P. Alken, M. Booth, and F. Rossi. Gnu scientific library. *Reference Manual edition*, 1, 2007.

[10] S. K. Lele. Compact finite difference schemes with spectral-like resolution. *Journal of Computational Physics*, 1992.

[11] S. Pirozzoli. On the spectral properties of shock-capturing schemes. *Journal of Computational Physics*, 219(2):489–497, 2006.

[12] J. H. Seo and Y. J. Moon. Linearized perturbed compressible equations for low mach number aeroacoustics. *Journal of Computational Physics*, 218(2):702–719, 2006.

[13] D. I. Shuman, S. K. Narang, P. Frossard, A. Ortega, and P. Vandergheynst. The emerging field of signal processing on graphs: Extending high-dimensional data analysis to networks and other irregular domains. *IEEE Signal Processing Magazine*, 30(3):83–98, May 2013.

[14] M. L. Shur, P. R. Spalart, and M. K. Strelets. Noise prediction for increasingly complex jets. part i: Methods and tests. *International journal of aeroacoustics*, 4(3):213–245, 2005.

[15] M. L. Shur, P. R. Spalart, and M. K. Strelets. Jet noise computation based on enhanced des formulations accelerating the rans-to-les transition in free shear layers. *International Journal of Aeroacoustics*, 15(6-7):595–613, 2016.

[16] C. K. Tam. *Computational aeroacoustics: a wave number approach*, volume 33. Cambridge University Press, 2012.

[17] C. K. W. Tam and J. C. Webb. Dispersion-relation-preserving finite difference schemes for computational acoustics. *Journal of Computational Physics*, pages 262–281, 1993.

[18] L. N. Trefethen. Group velocity in finite difference schemes. *SIAM review*, 24(2):113–136, 1982.

[19] F. X. Trias, O. Lehmkuhl, A. Oliva, C. D. Pérez-Segarra, and R. Verstappen. Symmetry-preserving discretization of navier–stokes equations on collocated unstructured grids. *Journal of Computational Physics*, 258:246–267, 2014.

[20] R. Vichnevetsky. Propagation through numerical mesh refinement for hyperbolic equations. *Mathematics and Computers in Simulation*, 23(4):344–353, 1981.